ELSEVIER

Journal of Neuroscience Methods 170 (2008) 294–299

JOURNAL OF NEUROSCIENCE METHODS

www.elsevier.com/locate/jneumeth

Short communication

Automated detection of intercellular signaling in astrocyte networks using the converging squares algorithm

Mahboubeh Hashemi [a], Marius Buibas [b], Gabriel A. Silva [a,b,c,*]

[a] *Department of Bioengineering, University of California, San Diego, La Jolla CA 92037, United States*
[b] *Department of Ophthalmology, University of California, San Diego, La Jolla CA 92037, United States*
[c] *Neurosciences Program, University of California, San Diego, La Jolla CA 92037, United States*

Received 20 September 2007; received in revised form 10 January 2008; accepted 10 January 2008

Abstract

Intercellular calcium waves in central nervous system astrocyte networks underline the principle mechanism of cell signaling in astrocyte syncsytiums, which putatively contribute to the modulation of neuronal signaling and metabolic regulation. In support of carrying out systems level analyses of astrocyte networks, we have optimized and validated the converging squares image segmentation algorithm to automatically detect the relative spatial locations of all cells in a visible network as a preliminary step towards analyzing the dynamics of astrocyte intracellular calcium transients, which are the signals that mediate intercellular calcium waves. We used the temporal derivatives of pixel intensities as the data source for the algorithm. The method works by converging progressively smaller squares until the signal peak is reached. It is robust to noise and performs comparably to manual cell signal identification, but is much faster and efficient. This is the first reported application of this algorithm to glial networks that we are aware of.

Keywords: Glia; Astrocytes; Cell signaling; Image analysis; Networks; Calcium waves; Calcium transients

1. Introduction

Ratiometric fluorescence techniques using ionic or voltage sensitive dyes permit investigation of functional physiology using epifluorescence microscopy at high spatial and temporal resolutions in large networks of both neurons and macroglia (Gobel et al., 2007; Yaksi and Friedrich, 2006). In particular, astrocyte syncsytiums in the central nervous system (CNS) putatively modulate neuronal physiology by modulating signaling and metabolic processes, for example, by regulating post-synaptic neurotransmitter concentrations or the release of vasoactive compounds (Piet et al., 2004; Takano et al., 2007). A ubiquitous but still poorly understood mechanism of signaling in astrocyte networks is intercellular calcium waves (ICW). Although we have a relatively clear understanding of the molecular and cellular details involved during signaling, their physiological and pathophysiological roles are not well understood. Intracellular calcium transients mediate intercellular signaling in astrocyte networks by regulating the intercellular diffusion of adenosine triphosphate (ATP) acting on P2Y purinergic receptors and the diffusion of inositol triphosphate (IP_3) through connexin hemichannel gap junctions (Scemes and Giaume, 2006). There is increasing interest in neuroscience in general and glial neurobiology in particular to better understand what ICW are doing and what effects they have on both neurons and glia. While qualitative recordings and measurements of ICW provide data for investigating qualitative molecular and cellular mechanisms, a full understanding of their physiological and/or pathophysiological roles will require further study of the dynamics of ICW quantitatively at the network level (i.e. at a functional level higher than the molecular and cellular details of ICW).

The first step towards any quantitative network analysis of ICW however necessitates identifying the relative spatial locations of and calcium transient activation events in individual astrocytes within a network. Though this can be done manually by going through a recorded movie sequence and identifying calcium transient activation events in individual cells, it is a tedious process that slows the progress of the analysis and is subject to

* Corresponding author at: UCSD Jacobs Retina Center, 9415 Campus Point Drive, La Jolla, CA 92037-0946, United States. Tel.: +1 858 822 4591.
E-mail address: gsilva@ucsd.edu (G.A. Silva).

0165-0270/$ – see front matter © 2008 Elsevier B.V. All rights reserved.
doi:10.1016/j.jneumeth.2008.01.013

operator error and subjectivity. Yet, it is a difficult process to automate due to the morphological heterogeneity of astrocytes and the spatiotemporal heterogeneity of the calcium responses themselves. Most existing cell segmentation imaging algorithms work well for cells which have regular and convex shapes, but are generally less reliable and accurate for cells which may overlap or have branch like projections, such as astrocytes. Furthermore, when using ionic-sensitive dyes, the signals are highly spatially and temporally variant, resulting in heterogeneous patterns of cell activation and deactivation that vary from cell to cell in a network. To address these issues, we have optimized the converging squares peak intensity finding algorithm (O'Gorman and Sanderson, 1983) for identifying and mapping calcium transient responses in two-dimensional astrocyte glial networks (e.g. for *in vitro* preparations or isolated planes of focus in *in situ* slice preparations). This approach is able to robustly and accurately detect dynamic calcium changes in individual cells, resulting in a protocol that efficiently automates the process for large astrocyte networks. This is the first reported application of the converging squares algorithms to glial networks that we are aware of.

2. Methods

2.1. Experimental preparations and imaging parameters and ranges

In vitro cultures of neonatal rat spinal cord astrocytes were incubated with fluo-4 calcium sensitive dye and were imaged using fluorescence microscopy, acquiring images at 16.7 Hz. An Olympus IX81 microscope and a Hamamatsu Orca ER camera were used to capture the images with 12-bit quantization at 100× magnification. Arbitrarily chosen cells were mechanically or pharmacologically stimulated with a micron-needle pipette and ICW imaged as they spread through the networks. Three image sequences were recorded, representing well over 2400 images and 100 detected cell signals.

We used a 10-frame lag to calculate the temporal derivative of sequences, effectively calculating the derivative after a 10-frame temporal averaging filter had been applied to sequence images. A 10-frame moving average was chosen because it took that many frames on average for the rising phase of calcium transient signals to reach their peak, which was the portion of calcium transients considered by the algorithm. The filtering was done to remove random fluctuations and noise on a shorter time scale then the physiological signal. Absolute intensity changes from baseline as a threshold indicator of a calcium transient event are not reliable because of the inter-cell variability in this parameter, which could putatively result in both false negative and false positive errors by the algorithm. For example, different cells can experience different indicator dye loading amounts that would result in different measured absolute fluorescence intensity values. Given this experimental constraint, we took a sustained relative increase in intensity (i.e. the first time derivative of the absolute intensity) over a 10-frame averaging window as our criteria to detect a signaling event. Because calcium transients associated with intercellular calcium waves are signaling events that are temporally rapid mediated by significant increase in cytosolic calcium, thresholding the derivative instead of the absolute level of fluorescence intensity provided a better indicator of the event and avoided non-signaling calcium changes which may have similar absolute changes in amplitude but which occur on slower time scales. In practical terms, our adaptation of the algorithm does not average this window first and then takes the derivative, it subtracts the intensity value at each pixel 10 frames apart, which due to commutative properties is mathematically equivalent to performing an averaging operation followed by taking a derivative.

To maximize temporal resolution, the camera's gain was set to its maximum value. A threshold value of 130 intensity units per 10 frames was chosen as an arbitrary value of cell activation, representing two standard deviations above baseline fluorescence levels. This value may depend on the cell type and experimental conditions, and should be appropriately chosen by the investigator to represent an appropriate cell activation event. Our chosen values were based on 8-bit quantization, but the value can easily be expressed as a relative change in fluorescence intensity as a $\Delta F/F$ percentage value, thereby thresholding cell signals above a certain percentage intensity change relative to background.

2.2. Implementation of the converging squares algorithm to astrocyte signaling networks

First introduced by O'Gorman and Sanderson (1983), the method works by tracking the signal centers through successive decreases in square size. A square region of specified image size is divided into four square sub-regions. The sub-region with the highest average intensity becomes the new region for subdivision. The process iteratively repeats itself until the region reaches one pixel in size, providing the peak of the initial region. Fig. 1 illustrates the process for a single astrocyte, and shows how progressive decreases in square size converge to the highest intensity pixel near the center of the cell.

In our implementation, we took the temporal derivative of the image sequence and clipped the signal to a lower bound of zero, essentially subtracting the intensity values of two frames:

$$I_t = \max(I(f+\delta) - I(f), 0)$$

where I_t is the intensity threshold t, $(f+\delta)$ and (f) are frames separated by some time δ, and $I(f+\delta)$ and $I(f)$ is their difference in intensity. Since only increases in $[Ca^{2+}]_i$ need be considered to detect activation events, negative intensity changes were disregarded and any negative values set to zero. A rapid positive increase in $[Ca^{2+}]_i$ indicated that a cell had received a signal and had actively responded. We used a selected threshold value, as discussed below, to establish this event. By thresholding the intensity change rather than absolute intensity values, we located only those cells that had been involved in signaling, which is usually a subset of the cells in a network and present in the field of view. Additionally, using the temporal derivatives obtained by subtracting image fields reduced systemic artifacts like uneven lighting and dead cells that might have had sustained elevated Ca^{2+} levels or autofluorescence which if mapped would contribute to false positive results.

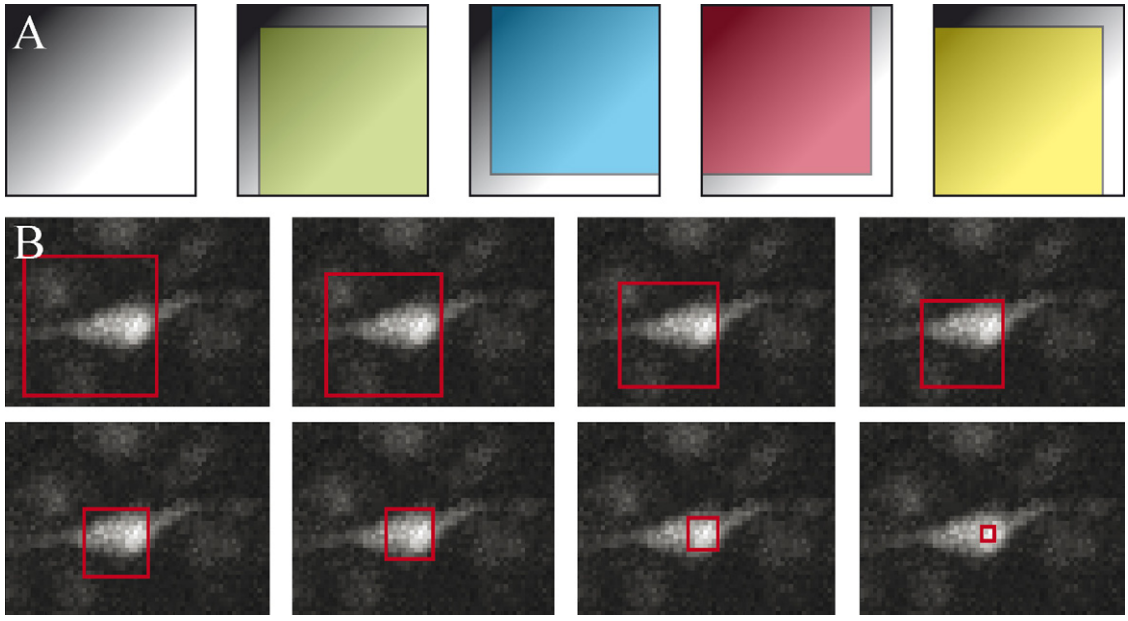

Fig. 1. Converging squares algorithm. (A) A square region of interest is selected (top left) and subdivided into four overlapping squares of smaller length (top row, colored squares). The square with the highest sum of pixel intensity values of the four becomes the new smaller square region of interest, and the procedure is repeated, reducing the square size until a single pixel is reached. (B) Application of the algorithm to a single astrocyte from an imaged sequence. An initial square placed around a cell converges to a single pixel centered on the region of highest intensity for the calcium-sensitive dye fluorescence. While the image is relatively noisy and there are numerous surrounding cells, the strongest signal peak is correctly detected and accurately localized.

For the converging squares algorithm, we chose an initial square size with a side length of 10 pixels. The sides of the square were shrunk by one pixel in each iteration, though this parameter can be increased for faster processing. The seed region for initial square placement occurred when a portion of pixels from the region were above the threshold. The algorithm was executed for each image, and peaks were aggregated for each frame in the sequence. The range of the square size parameter was chosen such that it was larger than the average size of one cell but smaller than the average area that contains two cells (which is based on the side of the square being smaller than the average distance between closest neighboring cells) so that the starting area of a square does not encompass more than one cell. Otherwise the algorithm will converge towards the more intense of the two cells and potentially miss the second cell altogether. A full discussion on thresholding criteria is system dependent and beyond the scope of this manuscript, but in our specific case we tested the observable absolute range of intensity changes, which varied from noise fluctuations at about 20 pixels per frame to the absolute maximum at around 130 pixels per frame.

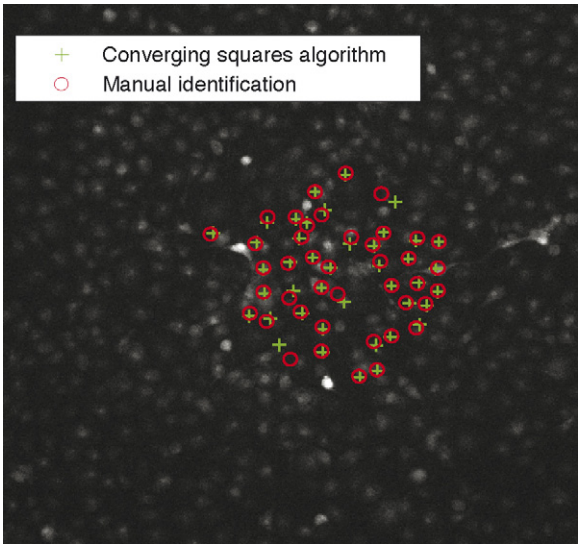

Fig. 2. Comparison of manual (crosses) and automated (circles) peak detection by the converging squares algorithm. For the algorithm, we used a square size of 10 pixels and a threshold of 80 pixels/frame (see text for details).

After the whole image sequence was completed, the combined peaks were clustered using the *k*-means clustering algorithm, which clusters objects by minimizing a squared error function (John et al., 2003) and a radius of 4-pixels. This step eliminated duplicate peaks and further refined peak location by averaging across multiple frames (Fig. 1B). All image processing was done in Matlab, implemented as an *m*-function that operates on a single image. All code can be obtained by contacting the corresponding author.

3. Results

To evaluate the efficiency of the algorithm, we compared the converging squares derived peaks with corresponding manually selected cell centroids (Fig. 2). While manual selection was performed on raw images, the converging squares method was executed on the temporal derivative of the images for a given threshold, resulting in a more stringent criterion for establishing a cell activation peak. Lowering the threshold parameter increased the number of cells that were detected

and slightly increased the overall error in comparison with manually selected cell activations. The threshold is an arbitrarily chosen parameter and must be appropriately chosen to establish the lower limit of Ca^{2+} fluorescence for a cell activation event. The initial square size was varied for the same dataset to understand the sensitivity of the seed region. This parameter is also arbitrary and should be initially chosen to be relatively close to the average cell size (see Section 2.2 above). Large square sizes will slow performance because the algorithm will take longer to converge and may miss cells altogether (false negatives), while small square sizes may result in multiple centroids being mapped for individual cells (false positives).

The average error distances of the automatically located peaks compared to manually located centroids, measured as the difference between manually selected and automatically detected centroids, were small and well within the margin of error of manual selection subjectivity. Furthermore, the error is small compared to the relative size of a cell of about 12–15 pixels at 10× magnification. For all datasets tested we evaluated square size values that on average were more than one cell length but less than two, while for the threshold we tested the observable absolute range of fluorescence intensity changes, which varied from noise fluctuations (at about 20 pixel intensity per frame) to an absolute maximum at around 130 pixel intensity per frame. Fig. 3 shows box plots for both square size and intensity threshold measured as a function of distance from the manually selected data for the same fields of view when holding the complimentary parameter constant at the value that yielded the closest results to the manually selected data (i.e. a threshold of 80 pixels per frame and square size of 10 pixels). For these optimal values, the automatically detected data displayed tight quartiles and maximum data value relative to the median, with error distances less than 5 pixels relative to manually selected data. Parameter values far from these optimums exhibited higher average errors and larger descriptive statistical distributions. In all cases, the number of outliers were small compared to the total number of cells being counted.

4. Discussion

While many methods and algorithms exist for cell localization and segmentation, few are robust against noisy data and irregular cell shapes. A number of cell segmentation methods exist, including some which have been applied to central nervous system cells, for identifying automated cell morphology (Bartels et al., 1996; Hamilton et al., 1998; Miller et al., 2002; Nedzved et al., 2005; Sharma and Sharma, 2004). These types of applications tend to be focused on automatically identifying pathological cells and tissues, such as neoplasms, and are a part of what is often called scanning cytometry, which is the development of fully automated microscopy not just for morphology or spatiotemporal functional signaling but for other applications as well, including for example the identification of cell types via biomarkers, antibodies, high throughput screening assays etc. (Adams et al., 2004; Binder, 2006; Bowen and Wylie, 2006; Green, 1990; Harnett, 2007; Kamentsky, 2001; Levenson and Mansfield, 2006; Lidke et al., 2003; Roman et al., 2002; Tarnok and Gerstner, 2002; Whimster et al., 1995). There is a relatively large body of work that has focused on scanning cytometry applications to neurons, such as the identification of specific neuronal subtypes via biomarkers and antibodies, gene expression, functional characterization of ion channels and anatomical identification (Aguila et al., 2006; Bingham et al., 2006; Blass-Kampmann et al., 1997; Crang et al., 2004; Dahlstrom et al., 1982; Ma and Cui, 2004; Mosch et al., 2006; Schild et al., 1995; Shepherd et al., 2005; Sureda et al., 1997; Verdaguer et al., 2002). However, these analyses are very different both methodologically and in their applications to the spatiotemporal detection of a second messenger during functional signaling events as, we describe here. There has been even less work done on glia in general or astrocytes in particular, which have only been described within the context of neurons (Mosch et al., 2006). Although some work has focused on the identification and quantitative spatial analysis of intercellular calcium waves at the cellular level in cardiac myocytes (Bray et al., 2007) and developing zebra fish (Ashworth and Bolsover, 2002; Gilland et al., 1999; Van der Linden et al., 2002; Webb and Miller, 2003), to the best

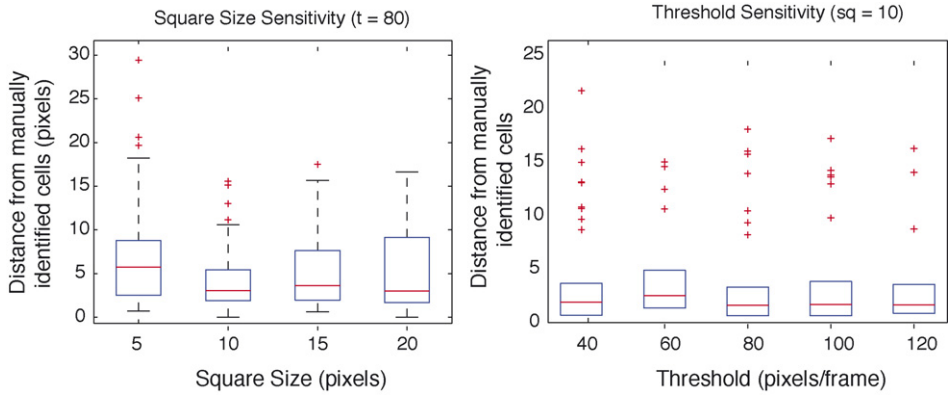

Fig. 3. Box plot summary statistics of initial square size variation and activation threshold sensitivity for automatically detected astrocytes compared to manually selected cells for the same field of view. For each plot, the complimentary parameter (i.e. square size or threshold) was fixed to its derived optimum as indicated, while the other parameter was varied. The figures show an optimal range for both parameters where the error difference between automated and manually selected cell identifications was minimal and within the subjective error range of manual selection.

of our knowledge there is no report describing the automated identification and quantitative spatiotemporal characterization of calcium transients or intercellular calcium waves in either glia or neurons. And although no method is as robust and adaptable as the human eye at identifying and segmenting shapes, this introduces subjectivity and over prolonged periods can increase the number of errors due to fatigue.

Yet, as argued above our understanding of the physiological role played by astrocytes in the CNS is ever increasing and the quantitative analyses of these cells will require an ability to map their functional signaling. The version of the converging squares algorithm presented here produces results that are very close to manual identification. It is also fast, taking about one second per image, which is important for analyzing large networks of cells over tens of seconds and even minutes. This method is robust to image noise, especially Gaussian noise from high gain settings on a CCD sensor (O'Gorman and Sanderson, 1983). Although a number of other signal detection methods could potentially be used for the automated spatiotemporal identification of intercellular signaling in astrocyte networks, our choice of the converging squares algorithm was primarily based on its robustness to noise and computational efficiency (O'Gorman and Sanderson, 1983). Its robustness to noise arises because the algorithm operates on whole regions at a time (i.e. squares) and not at individual points such as pixels, which in practical terms means that the data does not have to be filtered. Its computational efficiency arises in part because signal levels for overlapping squares (i.e. overlapping areas in the field of view) being considered by the algorithm do not need to be re-computed for different iterations.

Finally, the algorithm can also work in multiple dimensions, and time can be used as the third dimension in an image sequence. In this case, instead of a diminishing square a diminishing cube would be used, with time as the z-axis. Extending the current two-dimensional implementation into three-dimensions will slow down the algorithm, but may be robust in localizing maximum signal intensities in both space and time across an imaged movie. In addition, the general method introduced here should be more broadly applicable to other glial cells and also potentially calcium or voltage sensitive dye imaging in neurons.

Acknowledgments

This work was supported by funds from NIH grant NINDS NS054736, and by a fellowship to M.B. from Hewlett Packard.

References

Adams CL, Kobets N, Meiklejohn GR, Millington OR, Morton AM, Rush CM, et al. Tracking lymphocytes in vivo. Arch Immunol Ther Exp (Warsz) 2004;52:173–87.

Aguila B, Roussel M, Jauzac P, Allouche S. High-purity selection and maintenance of gene expression in human neuroblastoma cells stably over-expressing GFP fusion protein. Application for opioid receptors desensitization studies. Brain Res 2006;1114:11–8.

Ashworth R, Bolsover SR. Spontaneous activity-independent intracellular calcium signals in the developing spinal cord of the zebrafish embryo. Brain Res Dev Brain Res 2002;139:131–7.

Bartels PH, Thompson D, Montironi R. Knowledge-based image analysis in the precursors of prostatic adenocarcinoma. Eur Urol 1996;30:234–42.

Binder SR. Autoantibody detection using multiplex technologies. Lupus 2006;15:412–21.

Bingham B, Kotnis S, McHendry-Rinde B, Shen R, Wood A, Kennedy JD. Laser scanning cytometry in the characterization of the proapoptotic effects of transiently transfected genes in cerebellar granule neurons. Cytometry A 2006;69:1114–22.

Blass-Kampmann S, Kindler-Rohrborn A, Deissler H, D'Urso D, Rajewsky MF. *In vitro* differentiation of neural progenitor cells from prenatal rat brain: common cell surface glycoprotein on three glial cell subsets. J Neurosci Res 1997;48:95–111.

Bowen WP, Wylie PG. Application of laser-scanning fluorescence microplate cytometry in high content screening. Assay Drug Dev Technol 2006;4:209–21.

Bray MA, Geisse NA, Parker KK. Multidimensional detection and analysis of Ca^{2+} sparks in cardiac myocytes. Biophys J 2007;92:4433–43.

Crang AJ, Gilson JM, Li WW, Blakemore WF. The remyelinating potential and *in vitro* differentiation of MOG-expressing oligodendrocyte precursors isolated from the adult rat CNS. Eur J Neurosci 2004;20:1445–60.

Dahlstrom A, Booj S, Goldstein M, Larsson PA. Cytofluorimetric scanning: a tool for studying axonal transport in monoaminergic neurons. Brain Res Bull 1982;9:61–8.

Gilland E, Miller AL, Karplus E, Baker R, Webb SE. Imaging of multicellular large-scale rhythmic calcium waves during zebrafish gastrulation. Proc Natl Acad Sci USA 1999;96:157–61.

Gobel W, Kampa BM, Helmchen F. Imaging cellular network dynamics in three dimensions using fast 3D laser scanning. Nat Methods 2007;4:73–9.

Green DK. Analysing and sorting human chromosomes. J Microsc 1990;159:237–44.

Hamilton PW, Bartels PH, Montironi R, Anderson NH, Thompson D, Diamond J, et al. Automated histometry in quantitative prostate pathology. Anal Quant Cytol Histol Int Acad Cytol Am Soc Cytol 1998;20:443–60.

Harnett MM. Laser scanning cytometry: understanding the immune system *in situ*. Nat Rev Immunol 2007;7:897–904.

John NM, Kabuka MR, Ibrahim MO. Multivariate statistical model for 3D image segmentation with application to medical images. J Digit Imaging 2003;16:365–77.

Kamentsky LA. Laser scanning cytometry. Methods Cell Boil 2001;63:51–87.

Levenson RM, Mansfield JR. Multispectral imaging in biology and medicine: slices of life. Cytometry A 2006;69:748–58.

Lidke DS, Nagy P, Barisas BG, Heintzmann R, Post JN, Lidke KA, et al. Imaging molecular interactions in cells by dynamic and static fluorescence anisotropy (rFLIM and emFRET). Biochem Soc Trans 2003;31:1020–7.

Ma J, Cui FZ. Measuring membrane potential and electric field of brainstem neurons *in vitro* by confocal microscopy. Brain Res 2004;13:84–90.

Miller DH, Barkhof F, Frank JA, Parker GJ, Thompson AJ. Measurement of atrophy in multiple sclerosis: pathological basis, methodological aspects and clinical relevance. Brain 2002;125:1676–95.

Mosch B, Mittag A, Lenz D, Arendt T, Tarnok A. Laser scanning cytometry in human brain slices. Cytometry A 2006;69:135–8.

Nedzved A, Ablameyko S, Oczeretko E. Extraction of nerve cells in images with herpetic infections. Roczniki Akademii Medycznej w Bialymstoku (1995) 2005;50:284–8.

O'Gorman L, Sanderson AC. The converging squares algorithm: an efficient multidimensional peak picking method. Proc IEEE Int Conf Acoustics, Speech, Sig Proc 1983;8:112–5.

Piet R, Vargova L, Sykova E, Poulain DA, Oliet SH. Physiological contribution of the astrocytic environment of neurons to intersynaptic crosstalk. Proc Natl Acad Sci USA 2004;101:2151–5.

Roman D, Greiner B, Ibrahim M, Pralet D, Germann PG. Laser technologies in toxicopathology. Toxicol Pathol 2002;30:11–4.

Scemes E, Giaume C. Astrocyte calcium waves: what they are and what they do. Glia 2006;54:716–25.

Schild D, Geiling H, Bischofberger J. Imaging of L-type Ca^{2+} channels in olfactory bulb neurones using fluorescent dihydropyridine and a styryl dye. J Neurosci Methods 1995;59:183–90.

Sharma R, Sharma A. Physiological basis and image processing in functional magnetic resonance imaging: neuronal and motor activity in brain. Biomed Eng online 2004;3:13.

Shepherd GM, Stepanyants A, Bureau I, Chklovskii D, Svoboda K. Geometric and functional organization of cortical circuits. Nat Neurosci 2005;8:782–90.

Sureda FX, Escubedo E, Gabriel C, Comas J, Camarasa J, Camins A. Mitochondrial membrane potential measurement in rat cerebellar neurons by flow cytometry. Cytometry 1997;28:74–80.

Takano T, Han X, Deane R, Zlokovic B, Nedergaard M. Two-photon imaging of astrocytic Ca^{2+} signaling and the microvasculature in experimental mice models of Alzheimer's disease. Ann N Y Acad Sci 2007;1097:40–50.

Tarnok A, Gerstner AO. Clinical applications of laser scanning cytometry. Cytometry 2002;50:133–43.

Van der Linden A, Verhoye M, Van Meir V, Tindemans I, Eens M, Absil P, et al. *In vivo* manganese-enhanced magnetic resonance imaging reveals connections and functional properties of the songbird vocal control system. Neuroscience 2002;112:467–74.

Verdaguer E, Pubill D, Rimbau V, Jimenez A, Escubedo E, Camarasa J, et al. Evaluation of neuronal cell death by laser scanning cytometry. Brain Res 2002;9:41–8.

Webb SE, Miller AL. Imaging intercellular calcium waves during late epiboly in intact zebrafish embryos. Zygote (Cambridge, England) 2003;11:175–82.

Whimster WF, Cookson MJ, Salisbury JR. 3D reconstruction and quantitation of pathological tissues. Pathologica 1995;87:279–85.

Yaksi E, Friedrich RW. Reconstruction of firing rate changes across neuronal populations by temporally deconvolved Ca^{2+} imaging. Nat Methods 2006;3:377–83.